# Multishocks in driven diffusive processes: Insights from fixed-point analysis of the boundary layers

Sutapa Mukherji*
*Department of Physics, Indian Institute of Technology, Kanpur 208 016, India*
(Received 3 August 2010; revised manuscript received 27 October 2010; published 23 March 2011)

Boundary-induced phase transitions in a driven diffusive process can be studied through a phase-plane analysis of the boundary-layer equations. In this paper, we generalize this approach further to show how various shapes including multishocks and downward shocks in the bulk particle density profile can be understood by studying the dependence of the fixed points of the boundary-layer equation on an appropriate parameter. This is done for a particular driven interacting particle system as a prototypical example. The present analysis shows the special role of a specific bifurcation of the fixed points in giving rise to different kinds of shocks.

DOI: 10.1103/PhysRevE.83.031129 PACS number(s): 64.60.−i, 05.60.Cd, 05.40.−a, 05.70.Ln

## I. INTRODUCTION

In a one-dimensional driven diffusive process [1,2], particles typically hop to neighboring sites with a bias in a specific direction. These are nonequilibrium processes in which there is a finite particle current due to the biased diffusion of particles. A simple case entails particles hopping in a specific direction obeying the mutual exclusion rule, according to which a site cannot be occupied by more than one particle and a hop to an occupied target site is not allowed. After being injected at one end of the lattice at a rate $\alpha$, particles hop across the lattice and reach the other end, where they are withdrawn at a rate $1-\gamma$. Other models exist where particles can have attractive or repulsive interactions in addition to the exclusion interaction [3,4].

All these systems exhibit interesting boundary-induced phase transitions for which the tuning parameters are the boundary rates, $\alpha$ and $\gamma$ [5,6]. In different phases, the average particle density has distinct constant values across the bulk of the lattice. These particle density profiles in different phases may also differ due to the different location and nature of the boundary layers. More features, such as the coexistence of high- and low-density regimes, are seen in systems where the particle number is not conserved in the bulk due to attachment and detachment of particles to and from the lattice [7,8]. In this coexistence phase (also known as a shock phase), the particle density profile has a jump discontinuity (shock) in the interior of the lattice from a low to a high density value. The slope and the number of such shocks in a density profile are related to the nature of the interparticle interactions that determine the fundamental current density relation [9,10]. Although this relation predicts the kind of shocks that can be seen [10] in the density profile, a systematic characterization of the phase transition and the phase diagram in the $\alpha$-$\gamma$ plane requires a detailed analysis of the relevant equations describing the dynamics in the steady-state [8,11,12]. Drawing analogies from the equilibrium phase transitions, first-order, critical [6,7], and tricritical [12] kinds of phase transitions have been observed so far in various driven diffusive models.

While characterizing the phase transitions, it is useful to study the variation of the height or the width of the boundary layers as $\alpha$ and $\gamma$ are changed. In a way, these boundary layers play important roles in deciding the "order parameter"–like quantities in these nonequilibrium phase transitions. Owing to their importance in describing phase transitions, the boundary layers for several interacting and noninteracting models have been studied using the techniques of boundary-layer analysis [13]. It is found that the system usually enters into a shock phase from a nonshock phase due to the deconfinement of the boundary layer from the boundary. This deconfinement can be described by a nontrivial scaling exponent associated with the width of the boundary layer [8]. For the pure exclusion case, except for a critical point, the transition from a nonshock to a shock phase is first order in nature since a shock of finite height is formed on the phase boundary. The height of the shock on the phase boundary decreases as one approaches the critical point along the phase boundary. At the critical point, the shock height is 0 on the phase boundary and it increases continuously as one proceeds away from the phase boundary farther into the shock phase. To visualize these features, it is beneficial to obtain the full solution for the density profile along with its boundary layer. Boundary-layer analysis is useful for this purpose since it allows us to generate a uniform approximation for solving the steady-state particle density equation across the entire lattice. This steady-state equation can be obtained from the large time- and length-scale limit (hydrodynamic limit) of the statistically averaged master equation that describes the particle dynamics in the discrete form. For the simple exclusion case, it is possible to obtain an analytical solution of the steady-state hydrodynamic equation for the entire density profile. This, however, may not be possible for more complex driven diffusive models.

A fixed-point analysis of the hydrodynamic equation turns [14] out to be general and useful, since it does not involve an explicit solution of the steady-state hydrodynamic equation. In particle conserving models, a boundary layer saturates to the constant bulk density profile asymptotically. As a consequence of this, it is expected that the fixed points of the boundary-layer equation match the bulk density values. In other words, a boundary layer, which is a solution of the boundary-layer equation, is a part of the flow trajectory of the equation flowing to the appropriate fixed point on the phase plane. Thus, to find out the values of the bulk densities in different phases, it is sufficient to determine the physically acceptable fixed points of the boundary-layer equation. As a result, the number of

*sutapam@iitk.ac.in

 

possible bulk phases is given by the number of these fixed points. Applying this method to a specific particle conserving two-species process [14], it is found that this system has three distinct bulk phases corresponding to three fixed points of the boundary-layer equations. In addition, it is possible to predict the nature of the phase transitions, locations of the boundary layers, etc., for this system. All these predictions match well with the results from numerical simulations [15].

In a particle nonconserving case, the density is not constant in the bulk, and therefore, the fixed points of the boundary layer do not provide the full profile since the details of the bulk dynamics is not considered in this approach. However, it is still useful to obtain the fixed points of the boundary-layer equations along with their stability properties to predict the possible shapes of the density profiles under different boundary conditions. In the present paper, we generalize the method of reference [14] to study a particle number nonconserving model where particles interact repulsively. Our aim is to extend the fixed-point analysis to a system with nonconstant bulk density. We show how this analysis helps us predict possible shapes of the density profiles under different boundary conditions and also understand the properties of different kinds of shocks present in the density profile. This particular model is chosen because its density profiles have certain nontrivial shapes that include double shocks and downward shock. The present analysis reveals that such shocks arise in the density profile due to a specific saddle-node bifurcation [16] of the boundary-layer fixed points.

The plan of the paper is as follows. In the following section, we describe the model. This section also contains brief discussions on the hydrodynamic approach, boundary-layer analysis and some of the known results. In Sec. III, we present the phase-plane analysis of the boundary-layer equation for the present model. There are separate subsections on the boundary-layer equation, its fixed points and the stability analysis of the fixed points. Section IV presents the predictions of the possible shapes of the density profile under different boundary conditions. In Sec. V, we summarize these in terms of a few general rules. Some special features related to the saturation of the shocks are also discussed in this section. We end the paper with a summary in Sec. VI. A few details on various types of shocks associated with the fixed point diagram are provided in the Appendix.

## II. MODEL

### A. Discrete description

The driven process that we consider here consists of a one-dimensional lattice of $N$ sites with lattice spacing $a$. Particles are injected at $i = 1$ at a rate $\alpha$ and withdrawn at $i = N$ at a rate $1 - \gamma$. Particles, obeying mutual exclusion, hop to the right at rates that depend on the occupancy of the neighboring site as

$$1100 \to 1010 \quad \text{at rate} \quad 1 + \epsilon, \tag{1}$$

$$0101 \to 0011 \quad \text{at rate} \quad 1 - \epsilon, \tag{2}$$

$$0100 \to 0010 \quad \text{at rate} \quad 1, \tag{3}$$

$$1101 \to 1011 \quad \text{at rate} \quad 1. \tag{4}$$

Here, $0 < \epsilon < 1$, and 1 (0) represents an occupied(unoccupied) site. For $\epsilon \neq 0$, there is an effective repulsion between the particles [3,4,10]. In addition, the number of particles is not conserved due to particle detachment, $1 \to 0$, at a rate $\omega_d$ and attachment, $0 \to 1$, at a rate $\omega_a$ at any site on the lattice. Particle attachment and detachment are equilibrium-like processes that do not give rise to any particle current.

### B. Hydrodynamic approach and a brief description of the boundary-layer analysis

The hydrodynamic approach is based on the lattice continuity equation, which equates the time evolution of the particle occupancy at a given site with the difference of currents across its two neighboring bonds. In the continuum description, the continuous time and space variables are $t$ and $x$, with the latter replacing, for example, the $i$th site as $i \to x = ia$. Upon doing a Taylor expansion of the statistically averaged continuum version of the lattice continuity equation in small $a$, one has the hydrodynamic equation

$$\frac{\partial \rho}{\partial t} + \frac{\partial J}{\partial x} + S_0 = 0 \tag{5}$$

for the averaged particle density $\rho(x,t)$. This equation has already been supplemented with the particle nonconserving parts

$$S_0 = -\Omega(\rho_L - \rho), \tag{6}$$

where $\rho_L = \frac{\omega_a}{\omega_a + \omega_d}$ and $\Omega = (\omega_a + \omega_d)N$. $\Omega$ is kept constant as $N \to \infty$ so that the total flux is comparable to the current. The current, $J(\rho)$, consists of a bulk current $j(\rho)$ and a diffusive current proportional to $\frac{\partial \rho}{\partial x}$ as

$$J = -\epsilon_0 \frac{\partial \rho}{\partial x} + j(\rho). \tag{7}$$

Here, $\epsilon_0$ is a small parameter proportional to $a$. The diffusive current part arises naturally as one retains terms up to $O(a^2)$ in the Taylor expansion. To determine the particle density, $\rho(x)$, in the steady state ($\frac{\partial \rho}{\partial t} = 0$), one has to solve the differential equation with appropriate boundary conditions. We consider the lattice ends to be attached to the particle reservoirs which maintain constant densities $\rho(x = 0) = \alpha$ and $\rho(x = 1) = \gamma$. The diffusive current part is crucial here since, due to its presence, the hydrodynamic equation becomes a second-order differential equation, and as a result we can obtain a smooth solution satisfying both the boundary conditions.

The simplest driven process is the one with only the exclusion interaction, that is, $\epsilon = 0$. In this case, the current density relation $j(\rho) = \rho(1 - \rho)$ is an exact one. The symmetric shape of the current about its maximum at $\rho = 1/2$ is a consequence of its invariance under particle-hole exchange $\rho \to 1 - \rho$. It is well understood that the phase diagram has low-density ($\rho < 1/2$ at the bulk), high-density ($\rho > 1/2$ at the bulk), and maximum current ($\rho = 1/2$ at the bulk) phases [6]. The particle-hole symmetry is retained in $\epsilon \neq 0$ models, although the current changes nontrivially. At $\epsilon = 1$, that is, for the extreme repulsion case, hops such as $0101 \to 0011$ are forbidden. The current, therefore, vanishes exactly at half-filling ($\rho = 1/2$), with the maximum current appearing

symmetrically for densities on the two sides of $\rho = 1/2$. The exact form of the current as a function of $\rho$ for arbitrary $\epsilon$ can be found using a transfer matrix approach [4] and it evolves from a single to a symmetric double-peak structure as $\epsilon$ grows beyond $\epsilon_J \approx 0.8$. A simple, analytically tractable form of the current with double peaks can be obtained by doing a double expansion of the exact current about $\epsilon = \epsilon_J$ and $\rho = 1/2$ [12]. This leads to the following form for the current

$$j(\rho) = (2r + u)/16 - \frac{r}{2}(\rho - 1/2)^2 - u(\rho - 1/2)^4, \quad (8)$$

where the constant term is chosen in such a way that $j(\rho) = 0$ for $\rho = 0$ or 1. We recover the noninteracting limit, $j(\rho) = \rho(1 - \rho)$, for $r = 2$ and $u = 0$. The double-peak shape appears for $r < 0$. In the entire analysis below, we consider $r$ to be a small negative parameter and $u > 0$.

For the boundary-layer analysis, it is important to consider the bulk part and the narrow boundary layers or the shock regions of the density profile separately. These boundary layers or shocks are formed over a narrow region of width $O(\epsilon_0)$ and they merge to the bulk density in the appropriate asymptotic limit. To study the boundary layer and its asymptotic approach to the bulk, one can rescale the position variable in (5) as $\tilde{x} = (x - x_0)/\epsilon_0$, where $x_0$ is the location of the center of the boundary layer. Hence, for a boundary layer satisfying the boundary condition at $x = 1$, we have $x_0 \approx 1$. For small $\epsilon_0$, the boundary layer approaches the bulk density in the $\tilde{x} \to -\infty$ limit and satisfies the boundary condition at $\tilde{x} = 0$. In terms of $\tilde{x}$, the steady-state hydrodynamic equation is

$$\frac{\partial^2 \rho}{\partial \tilde{x}^2} - \frac{\partial j}{\partial \tilde{x}} - \epsilon_0 S_0 = 0. \quad (9)$$

Since $\epsilon_0$ is a small parameter, the effect of the particle nonconserving term, $S_0$, on the boundary layer is negligible. As a result, the total current $J = j(\rho) - \frac{\partial \rho}{\partial \tilde{x}}$ is constant across the boundary-layer. A shock, therefore, can be represented by a horizontal line connecting two densities in the $j$-$\rho$ plane as shown in Fig. 1. For an upward shock ($\frac{\partial \rho}{\partial \tilde{x}} > 0$), this line lies below the $j(\rho)$ curve and the reverse is true for a downward shock ($\frac{\partial \rho}{\partial \tilde{x}} < 0$). As a result, while for $r > 0$, only upward shocks are possible, for $r < 0$, downward shocks and double shocks can also be found. Double shocks can be represented by two horizontal lines on the $j$-$\rho$ plane below the two peaks in $j(\rho)$.

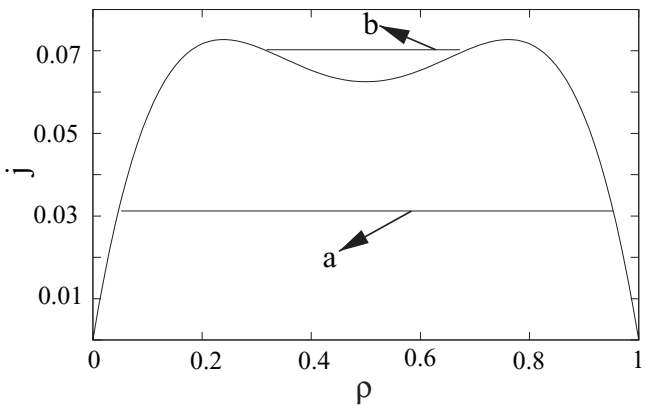


FIG. 1. Current $j$ is plotted as a function of $\rho$. Lines a and b represent an upward and a downward shock, respectively.

To zeroth order in $\epsilon_0$, the final boundary-layer equation is

$$\frac{\partial^2 \rho}{\partial \tilde{x}^2} - \frac{\partial j}{\partial \tilde{x}} = 0. \quad (10)$$

In the boundary-layer language, the solution of this equation is known as the inner solution. To obtain the bulk part of the density profile, one can ignore the diffusive current part in $J$ for small $\epsilon_0$. The steady-state equation that gives the bulk part of the density profile is

$$\frac{dj}{dx} + S_0 = 0. \quad (11)$$

The solution of this equation for the bulk part of the profile is known as the outer solution. These inner and outer solutions contain several integration constants which are fixed by the boundary conditions and other matching conditions of the boundary layer and the bulk under various limits. Since the slope of the outer solution is obtained from

$$\frac{d\rho}{dx} = -S_0 \Big/ \frac{dj}{d\rho} \quad (12)$$

for a given $\rho$, the slope depends crucially on the signs of $(\rho_L - \rho)$ and $\frac{dj}{d\rho}$. For the analysis below, we consider $\rho_L$ to be large and $\alpha$ and $\gamma$ to be much smaller than $\rho_L$.

### C. Known results

The double-peak structure of the current-density relation leads to two maximum-current and one minimum-current phase in the phase diagram of the particle conserving repulsion model [4]. In the maximum- and minimum-current phases, the bulk density values are those at which the current attains its maximum and minimum values, respectively. With these new phases, the phase diagram for this model becomes more complex than its noninteracting counterpart.

Combining the techniques of boundary-layer analysis and the results from numerical solutions, the phase diagram has been obtained for the particle nonconserving repulsion model [12]. The phase diagram has a lot of interesting features including a tricritical point at $r = 0$. In the $\alpha$-$\gamma$-$r$ phase diagram, this is a special point where two critical lines meet. It has been found that three different phase diagrams are possible for $r > 0$, $r = 0$, and $r < 0$. For $r > 0$, the current-density plot is symmetric around $\rho = 1/2$, with a maximum at $\rho = 1/2$. The nature of the phase diagram is qualitatively similar to the mutually exclusive case with one single critical point. For $r < 0$, with a double-peak structure of the current-density plot, the phase diagram is more complex, with more than one critical point and three different shock phases, with the density profile having a single upward shock, double upward shocks, and one upward and one downward shock [10,12]. Qualitatively, the phase diagrams for $r = 0$ and $r < 0$ appear as shown in Fig. 2 (see Ref. [12] for more details on the phase boundaries and associated exponents). Density profiles with double shocks or a downward shock are shown and discussed in detail in Sec. IV C.

The low-density peak can give rise to a low-density upward shock [$\rho(x) \leqslant 1/2$ in the shock part] in the density profile. A

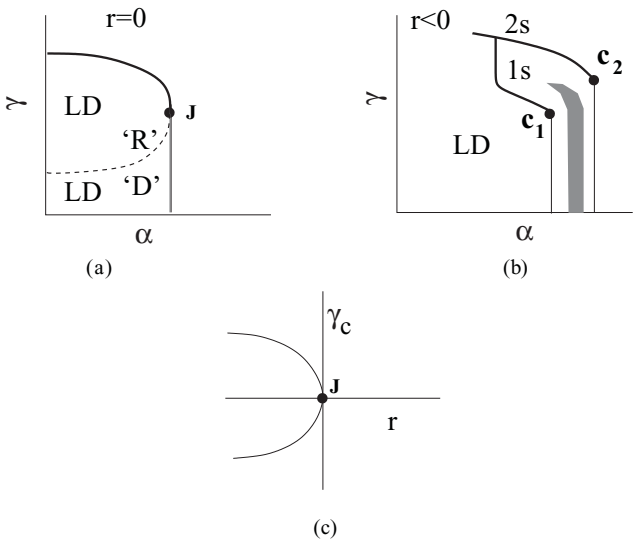


FIG. 2. Qualitative phase diagrams for different values of $r = \epsilon - \epsilon_J$. LD represents the low-density phase with the boundary layer at $x = 1$. Thick and thin solid lines represent first-order and continuous phase transitions, respectively. Dashed line represents a surface transition line across which the boundary layer near $x = 1$ changes from a particle-rich (R) one to a particle-depleted (D) one. $c_1$ and $c_2$ represent critical points. (a) Tricritical point, J. (b) Shaded area represents a region where the density profile has a downward shock. The double-shock phase (2s) appears above the single-shock (1s) phase. The surface transition line is not shown explicitly here. (c) Merging of critical lines (critical points $c_1$ and $c_2$ in $\gamma$-$\alpha$ plane) in the $\gamma$-$r$ plane. The separation between the two critical lines $\Delta\gamma$ vanishes with a specific scaling exponent as $r \to 0$ from below. There is another critical line through J for $r > 0$.

single shock of this kind can be represented by a horizontal line in the $j$-$\rho$ plane below the low-density peak. The critical point corresponds to a situation where the horizontal line reaches the peak position implying a shock of zero height. The second distinct critical point, which involves both the peaks of the current-density plot, is not symmetrically related to this. The density profile, here, has two upward shocks, in which one is a low-density shock and one is a high-density shock with $\rho > 1/2$. The low-density shock, in this case, has the maximum height, with its high-density end saturating to $\rho = 1/2$. The high-density shock, which is due to the high-density peak of the current-density plot, can be of varying height. The critical point corresponds to the special point where this high-density shock has zero height. In addition to these regions, there are regions in the phase diagram, where density profiles with a downward shock or a single, symmetric upward shock are found.

In view of the symmetry of the $j$-$\rho$ diagram, it is natural to expect the two critical points to be related through this symmetry. Previous work, however, shows that the shapes of the density profiles are not related through this symmetry near these two special points. Unlike the low-density shock, the high-density shock in the density profile is always accompanied by a low-density shock of maximum height. The following analysis clearly reveals the reasons behind such asymmetries.

## III. PHASE-PLANE ANALYSIS OF THE BOUNDARY-LAYER EQUATIONS

In this section, we determine the fixed points of the boundary-layer equation and their stability properties. These fixed points are the special points to which the boundary-layer solution saturates in the appropriate limit. The knowledge about the fixed points and their stabilities can, therefore, be used to our advantage to find out, for example, the bulk densities to which a shock or a boundary layer saturates at its two edges.

### A. Boundary-layer equation

Substituting the expression for $j(\rho)$ as given in Eq. (8) and integrating the boundary-layer equation, (10), once, we have

$$\frac{d\rho_1}{d\tilde{x}} + \frac{r}{4}\rho_1^2 + \frac{u}{8}\rho_1^4 = C_0. \tag{13}$$

Here $\rho_1 = 2\rho - 1$ and $C_0$ is the integration constant. The saturation of the boundary layer to the bulk density, $\rho_{1b}$, is ensured by choosing the integration constant as

$$C_0 = \frac{r}{4}\rho_{1b}^2 + \frac{u}{8}\rho_{1b}^4. \tag{14}$$

As per Eq. (8), $C_0$ is related to the excess current (positive, negative, or 0) measured from $\rho = 1/2$ (half-filled case). The entire following analysis is done in terms of $\rho_1$, for which the boundary conditions are $\rho_1(x = 0) = \alpha_1 = 2\alpha - 1$ and $\rho_1(x = 1) = \gamma_1 = 2\gamma - 1$.

### B. Fixed points

$C_0$ can be plotted for various $\rho_{1b}$, from $-1$ to 1. For $r < 0$, $C_0$ has a symmetric double-well structure around $\rho_{1b} = 0$ (see Fig. 3). The fixed points, $\rho_1^*$, in Eq. (13), are the solutions of the algebraic equation

$$\frac{u}{8}\rho_1^4 + \frac{r}{4}\rho_1^2 - C_0 = 0. \tag{15}$$

In general, there are four possible solutions for the fixed point as

$$\rho_1^* = \pm\left[\frac{|\, r \,| \pm\sqrt{r^2 + 8C_0u}}{u}\right]^{1/2}. \tag{16}$$

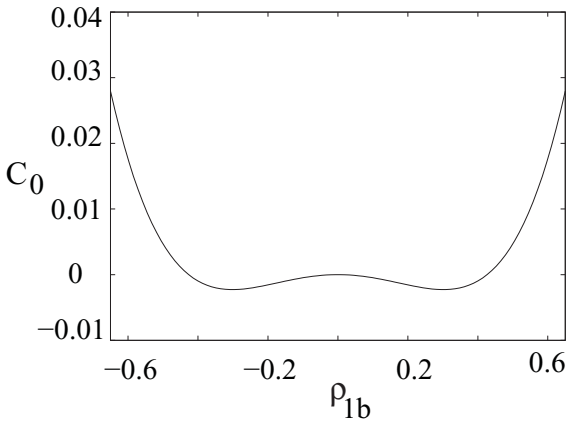


FIG. 3. $C_0$ plotted as a function of $\rho_{1b}$, with $r = -0.2$ and $u = 2.2$.

The value of $C_0$ depends on $\rho_{1b}$, the bulk density to which the boundary-layer solution saturates. As a consequence, for a given $C_0$, the corresponding $\rho_{1b}$ is always a fixed point. For the same $C_0$, there are, however, other fixed points, which are determined from Eq. (16). Hence, from the information about one saturation density, $\rho_{1b}$, the other saturation density of the shock can always be determined. The approach to various fixed points must, of course, be consistent with their stability properties. These stability properties of various fixed points are discussed in Sec. III C, below.

If $C_0$ is positive, there can be only two real fixed points of opposite signs. The positive and negative fixed points, denoted $\rho^*_{1\pm}$, respectively, are

$$\rho^*_{1\pm} = \pm\left[\frac{|\,r\,| + \sqrt{r^2 + 8C_0u}}{u}\right]^{1/2}. \tag{17}$$

If $C_0 < 0$, there are four fixed points for $\rho_{1b}$. In all these cases, the fixed points are symmetrically located on either side of the origin. The positive $\rho_1$ fixed points are

$$\rho^*_{1,2+} = \left[\frac{|\,r\,| \pm \sqrt{r^2 - 8\,|\,C_0\,|\,u}}{u}\right]^{1/2}, \tag{18}$$

and the negative $\rho_1$ fixed points are

$$\rho^*_{1,2-} = -\left[\frac{|\,r\,| \pm \sqrt{r^2 - 8\,|\,C_0\,|\,u}}{u}\right]^{1/2}. \tag{19}$$

Here, the subscripts 1 and 2 correspond to the plus and minus signs inside the bracket, respectively. It is important to note that there is no real fixed point for $C_0 < -\frac{r^2}{8u}$. As $C_0$ approaches this value from above, the pair of fixed points on the positive and negative sides approach each other and they merge at $C_0 = -\frac{|r|^2}{8u}$. At this special value, the fixed points are $\rho^{*\pm}_{1m} = \pm(\frac{|r|}{u})^{1/2}$. For $C_0 = 0$, there are three fixed points, $\rho^*_1 = 0$ and $\rho^{*\pm}_{10} = \pm(\frac{2|r|}{u})^{1/2}$.

Numerical values of the fixed points for some special values of $C_0$ with $r = -0.2$ and $u = 2.2$ are mentioned below. For $C_0 = 0$, the nonzero fixed points are $\rho^{*\pm}_{10} = 0$ and $\pm 0.426$. For these values of $r$ and $u$, no real fixed points are present if $C_0 < -\frac{r^2}{8u} = -0.00227$. At this special value of $C_0$, the two fixed points are $\rho^{*\pm}_{1m} = \pm 0.30151$.

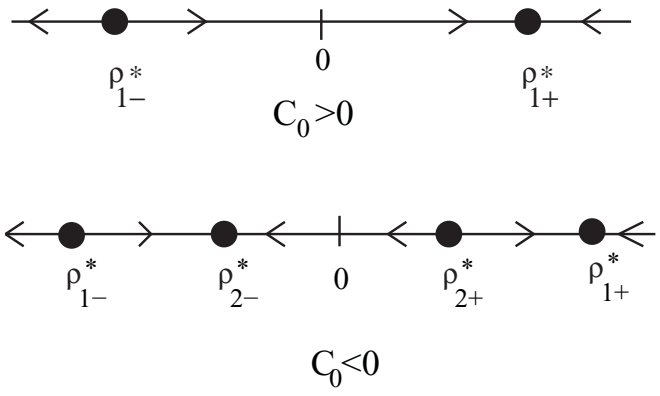


FIG. 4. Flow behavior of fixed points.

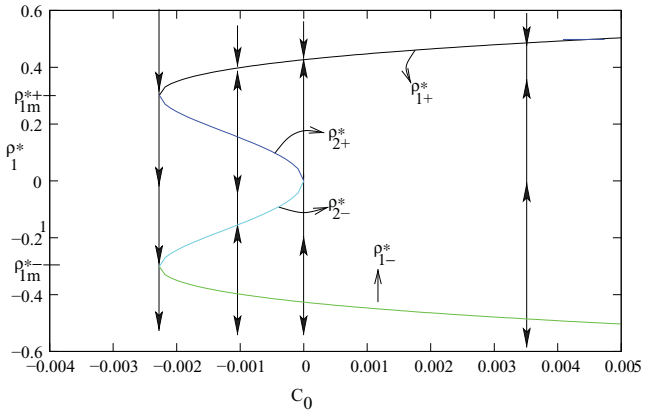


FIG. 5. (Color online) Fixed points are plotted for different values of $C_0$ with $r = -0.2$ and $u = 2.2$. $\rho^*_{1\pm}$ and $\rho^*_{2\pm}$ are different fixed points mentioned in the text. Four different parts of the two-lobed curve correspond to four different fixed points $\rho^*_{1\pm}$ and $\rho^*_{2\pm}$ as given in Eqs. (18) and (19).

### C. Stability analysis of the fixed points

For $C_0 > 0$, a linearization of Eq. (13) around the fixed points with $\rho_1 = \rho^*_1 + \delta\rho_1$ leads to the following stability equation:

$$\frac{d\delta\rho_1}{d\tilde{x}} = \frac{-\sqrt{|\,r\,|^2 + 8uC_0}}{2}\rho^*_1\delta\rho_1. \tag{20}$$

This implies that the fixed points $\rho^*_{1+}$ and $\rho^*_{1-}$ are, respectively, stable and unstable.

Similarly, for $C_0 < 0$, the general stability equation is

$$\frac{d\delta\rho_1}{d\tilde{x}} = \frac{\rho^*_1}{2}\,\delta\rho_1\big(|\,r\,| - u\rho^{*2}_1\big). \tag{21}$$

The flow around the fixed points can be obtained by substituting the explicit expressions of the fixed points. Figure 4 shows the stability properties of various fixed points for $C_0 > 0$ and $C_0 < 0$.

The stability property of the $\rho^*_1 = 0$ fixed point for $C_0 = 0$ and the pair of fixed points for $C_0 = -\frac{r^2}{8u}$ cannot be determined from the linear analysis. However, the flow around the fixed points can be predicted from the continuity of the flow behavior as $C_0$ approaches these special values. Fixed points, their stability properties, and how the fixed points change with $C_0$ are all shown in Fig. 5. As the diagram shows, the special value $C_0 = -\frac{r^2}{8u}$ corresponds to a saddle-node bifurcation [16] at which two pairs of stable and unstable fixed points appear.

## IV. PREDICTIONS ABOUT THE SHAPES OF THE DENSITY PROFILES

Based on Fig. 5, we attempt to predict possible shapes of the density profiles for given boundary conditions $\alpha_1$ and $\gamma_1$. We consider only a few pairs of boundary conditions, and based on this, we make certain general predictions in the next section. The basic strategy for drawing the density profile is as follows. We first need to mark $\alpha_1$ and $\gamma_1$ on the $\rho^*_1$ axis of the $C_0$-$\rho^*_1$ plane. Starting with either of the boundary conditions, we change $\rho_1$, along the curve in Fig. 5 in such a way that we reach the other boundary condition at the end of our move. While doing so, we may allow a discontinuous variation of $\rho_1$ along

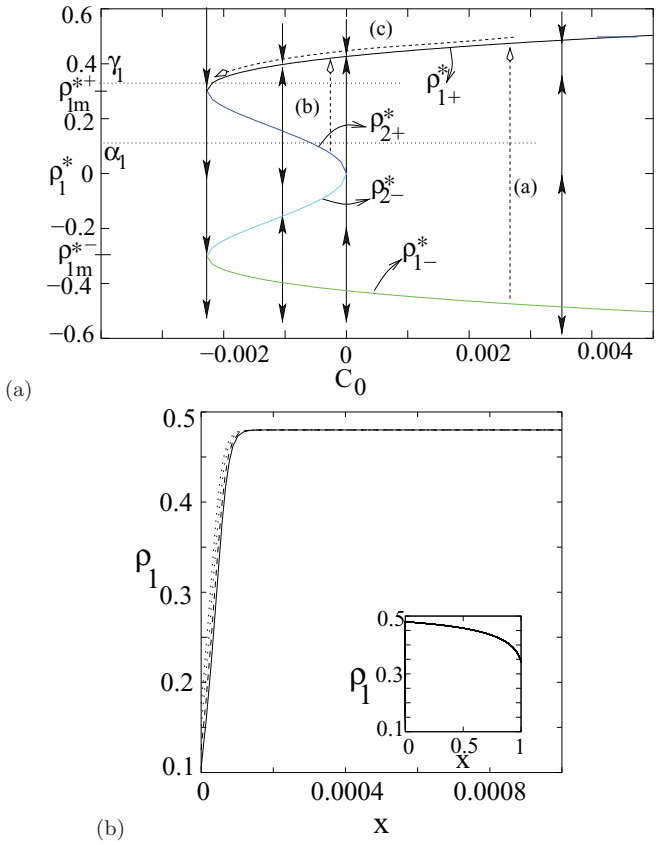


FIG. 6. (Color online) (a) Possible variations of density as one moves along the density profile from the $x = 0$ end are shown on the $C_0$-$\rho_1^*$ plane. Dashed lines or curves with open arrows show the variation of the density. Open arrows point in the direction of increasing $x$. Dotted lines mark the boundary conditions $\alpha_1$ and $\gamma_1$. Solid lines with arrows are the flow trajectories of the fixed points. (b) Numerical solutions for density $\rho_1$ for various $\alpha_1$ with $\gamma_1 = 0.34$. Inset: A view of the entire density profile. From a zoom-in view of the density profile near $x = 1$, it can be seen that the profile has no boundary-layer near $x = 1$.

a vertical constant-$C_0$ line, provided that it does not violate the flow property. Such a discontinuous change in $\rho_1$ appears in the form of a shock or a boundary layer in the density profile. The dashed, vertical lines in Fig. 6(a), for example, are the constant-$C_0$ lines along which the density may change. Such a dashed line, therefore, represents a boundary layer or a shock in the density profile. Two densities at which a shock or a boundary layer saturates are those at which a particular constant-$C_0$ line, representing a shock or a boundary layer, intersects the curves. These densities, at which a shock saturates on its left and right, are denoted $\rho_{1l}$ and $\rho_{1r}$, respectively, in the following. This method, however, sometimes leaves us with different options for the density profile. All these possibilities are shown on the $C_0$-$\rho_1^*$ plane for each pair of boundary conditions individually.

### A. Density profiles with only boundary layers

Suppose we consider a situation where $\alpha_1$, $\gamma_1 > 0$ with $\alpha_1 < \rho_{1m}^{*+}$ and $\gamma_1 > \rho_{1m}^{*+}$. It is possible that the density profile has a particle-depleted boundary layer ($\frac{d\rho_1}{dx}\,|_{x=0} > 0$) at $x = 0$ satisfying the boundary conditions $\rho_1(x = 0) = \alpha_1$. This boundary layer can be represented by a vertical line similar to line (a) in Fig. 6(a). This is consistent with the flow property that suggests the approach of the boundary layer to the fixed point $\rho_{1+}^*$ as $\tilde{x} \to \infty$. On the other hand, in the $\tilde{x} \to -\infty$ limit, which corresponds to the unphysical negative $x$ region, the boundary layer saturates to the unstable fixed point $\rho_{1-}^*$. After the boundary layer, the density may decrease continuously along line (c) on the $\rho_{1+}^*$ branch and satisfies the boundary condition, $\rho_1(x = 1) = \gamma_1$. There can be another possibility where the particle-depleted boundary layer at $x = 0$ is represented by a vertical line similar to line (b) joining the fixed points $\rho_{2+}^*$ and $\rho_{1+}^*$. The boundary condition at $x = 1$ is again satisfied by a decreasing density part parallel to line (c). For this to be possible the condition $\gamma_1 < \rho_{10}^{*+}$ is required. These two possibilities are distinct due to distinctly different values of $C_0$. This shows the crucial role played by $C_0$ in deciding the density profile. Numerical solutions of the full steady-state hydrodynamic equation presented in Fig. 6(b) show the boundary layers saturating to a bulk density $\rho_{1b} \approx 0.48$. This implies that the boundary layers are indeed represented by a-type vertical lines.

Next we consider $\alpha_1, \gamma_1 > 0$, with $\alpha_1 > \rho_{1m}^{*+}$ and $\gamma_1 < \rho_{1m}^{*+}$. In this case too, the density profile can satisfy the boundary condition at $x = 0$ through a boundary layer that can be represented by a line similar to line (a) in Fig. 7(a). This would be a particle-depleted boundary layer at $x = 0$. To satisfy the other boundary condition, the density should decrease till $\rho_{1m}^{*+}$ along path (b) on the $\rho_{1+}^*$ branch and then satisfy the right boundary condition through a particle-depleted boundary layer along line (c) in Fig. 7(a). The boundary condition at $x = 0$ can also be satisfied by vertical lines coming from above the $\rho_{1+}^*$ branch leading to particle-rich boundary layers ($\frac{d\rho_1}{dx}\,|_{x=0} < 0$) at $x = 0$. These lines could be a′-type lines in Fig. 7(a) satisfying the boundary condition $\alpha_1'$. Both particle-depleted and particle-rich boundary layers are present in the density profiles in Fig. 7(b) obtained by solving the full steady-state hydrodynamic equation numerically.

### B. Density profiles with upward shocks

With $\gamma_1 > \rho_{1m}^{*+}$ and $\alpha_1$ large negative, possible shapes of the density profile can be of the following kinds. We start with $\rho_1(x = 0) = \alpha_1$. $\rho_1$ decreases continuously along the $\rho_{1-}^*$ branch along the dashed line (a) in Fig. 8(a). After this part, an upward shock, represented by a vertical line similar to either (b) or (d) appears. In the latter case, the dashed line (a) should be extended until it reaches the low-density end of line (d). If the shock is represented by line (b), it is a large shock, symmetric about $\rho_1 = 0$. In the second case, the shock is a low-density shock, with the saturation densities being $\rho_{1r} = 0$ and $\rho_{1l} = \rho_{10}^{*-}$. If the density approaches the $\rho_{1+}^*$ branch after the large shock, the boundary condition at $x = 1$ can be satisfied subsequently by a decrease in density along line (c) on this branch. If the shock is of the line (d) kind, the density has to change further to satisfy the right boundary condition. Upon reaching the $\rho_1 = 0$ value, the density may change along the $\rho_{2-}^*$ or the $\rho_{2+}^*$ branch. The flow around $\rho_1^* = 0$, however, suggests that the density variation only along the $\rho_{2+}^*$ branch (path e in Fig. 8) is possible. The continuously increasing part along path e is then followed by another upward

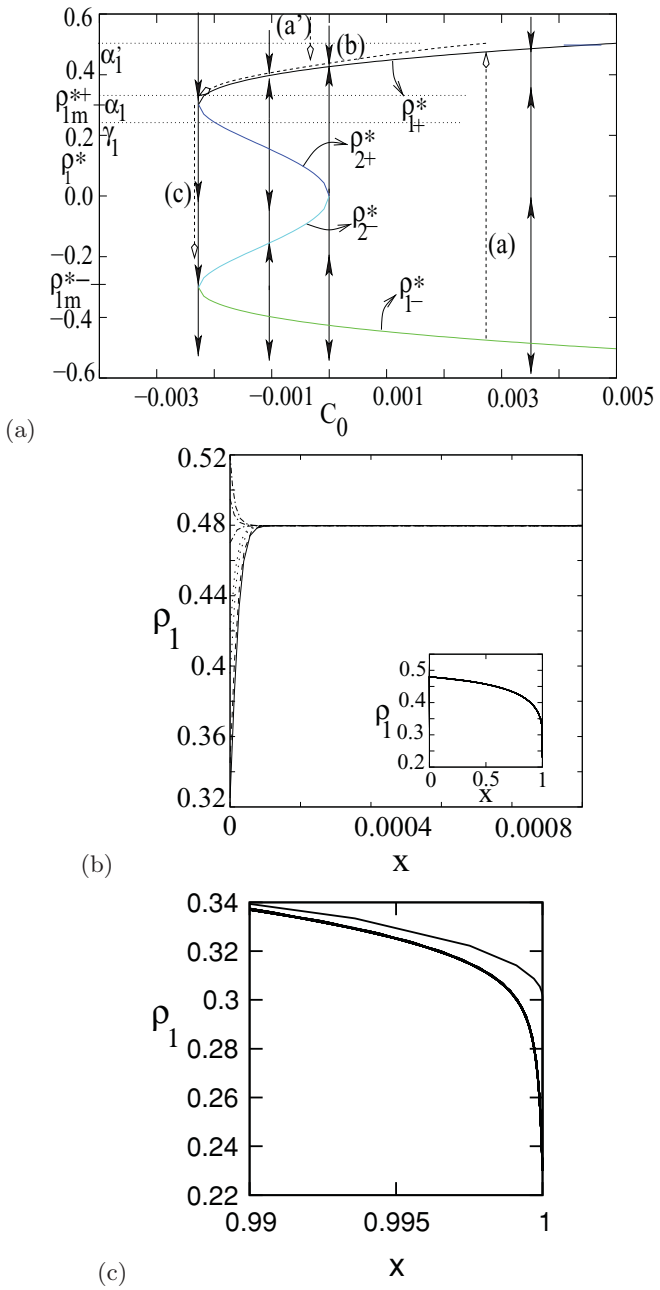


FIG. 7. (Color online) (a) Same as Fig. 6(a) except that here we explicitly show possible density variations for two different left boundary conditions, specified by $\alpha_1$ and $\alpha_1'$. (b) Numerical solutions for $\rho_1(x)$ for various $\alpha_1$ with $\gamma_1 = 0.23$. Zoom-in view of boundary layers near $x = 0$. Inset: Entire density profile over the entire lattice. (c) Zoom-in view of the same density profiles near $x = 1$, showing the particle-depleted boundary layers near $x = 1$.

shock, given by line (f), taking the density to the $\rho^*_{1+}$ branch. The boundary condition is then satisfied by a continuously decreasing part along a c-type line. Numerical solutions in Fig. 8(b) are consistent with these predictions.

### C. Density profiles with downward shocks

We next consider the case $\rho^{*-}_{1m} < \gamma_1 < 0$, with $\alpha_1$ increasing from large negative values. Here we specifically

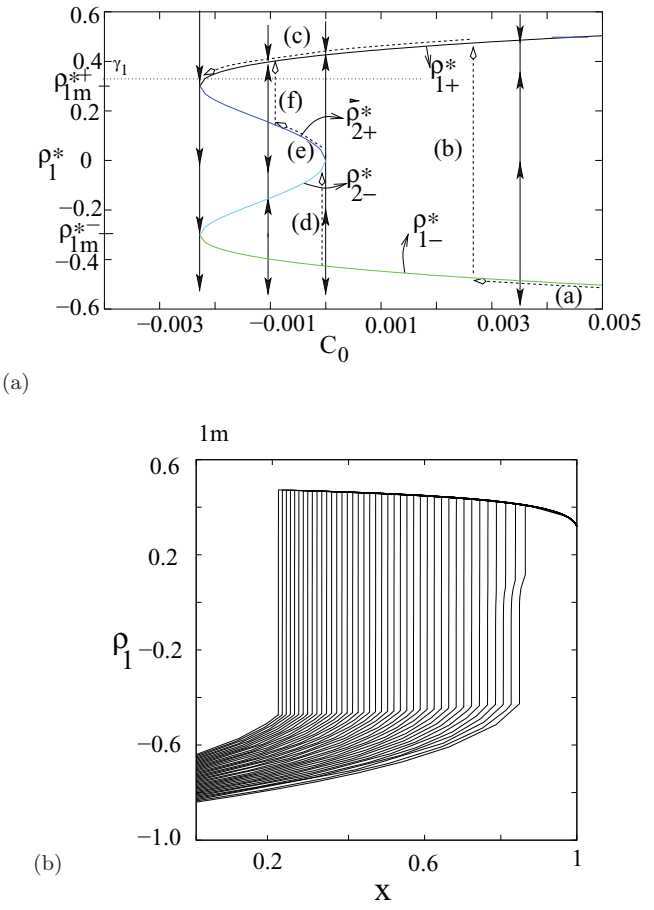


FIG. 8. (Color online) (a) Same as Fig. 6(a). (b) Plot of density profiles $\rho_1(x)$ for various large negative values of $\alpha_1$ with $\gamma_1 = 0.32$. No boundary layer is formed at $x = 0$ or $x = 1$. A few density profiles toward the right have double shocks.

mention how the density profile changes as $\alpha_1$ is changed, keeping $\gamma_1$ fixed. In the process, we observe how a density profile with a downward shock appears. Let us assume that our starting $\alpha_1$ lies somewhere on the $\rho^*_{1-}$ branch. $\rho_1$ increases from $\rho_1(x = 0) = \alpha_1$ along the $\rho^*_{1-}$ branch until it reaches the boundary $x = 1$. This continuously increasing part is represented by line (1a) in Fig. 9(a). The density, then, satisfies the right boundary condition through a boundary layer which can be, for example, represented by a vertical line like (1b) in Fig. 9(a). This line takes the solution from the unstable fixed point $\rho^*_{1-}$ to the stable fixed point $\rho^*_{1+}$. Since the vertical line (1b) passes through $\gamma_1$ before reaching the $\rho^*_{1+}$ branch, the boundary layer satisfies the boundary condition before saturating to the positive fixed point, $\rho^*_{1+}$. The boundary layer at $x = 1$ is, therefore, a part of this vertical constant-$C_0$ line.

As $\alpha_1$ is increased slightly, the route of the density along the $\rho^*_{1-}$ branch remains the same, but this time the density reaches a higher value than the previous $\alpha_1$ case before increasing sharply as a boundary -layer satisfying the boundary condition at $x = 1$. As $\alpha_1$ is increased further, for a given $\alpha_1$, the continuously increasing part of the profile reaches the low-density end of line (2b). After this, there is a shock in the density profile of the line (2b) kind. This is a low-density shock that takes the density to $\rho^*_1 = 0$. If this jump is near the

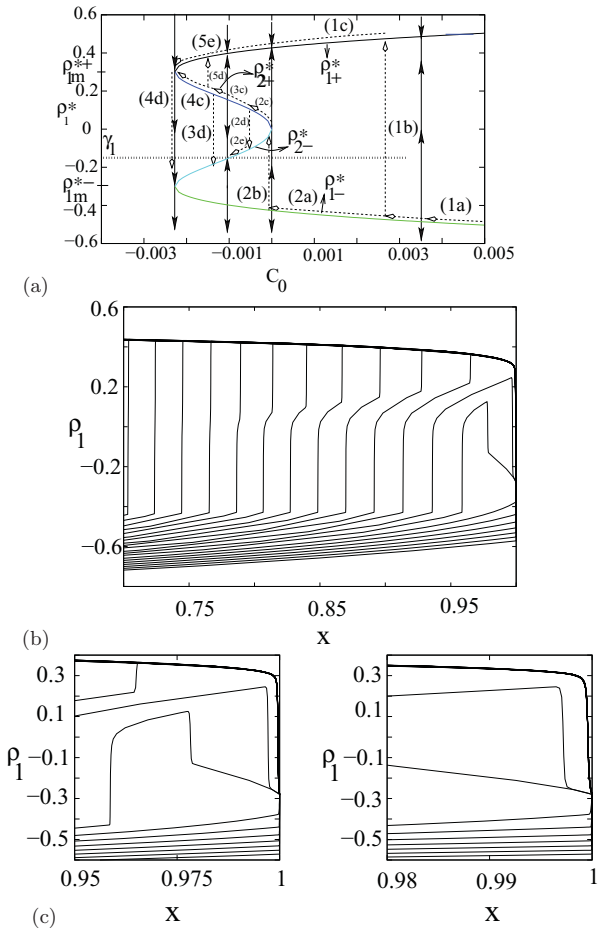


FIG. 9. (Color online) (a) Trajectory of the density on the $C_0$-$\rho_1$ plane. Five possible trajectories are shown, distinguished by different numbers. The alphabetical sequence represents the variation of the density along increasing $x$. (b) Plot of density profiles $\rho_1(x)$ for various $\alpha_1$ values with $\gamma_1 = -0.28$. (c) Zoom-in views of the boundary layers of the density profiles in (a) near $x = 1$.

boundary, the shock actually becomes a boundary layer that can help the density satisfy the boundary condition at $x = 1$. However, if this discontinuity is in the bulk, it is an upward low-density shock. In the case of a shock in the bulk, the density increases further along the $\rho^*_{2+}$ branch (path 2c in Fig. 9). The boundary condition, however, demands a decrease in $\rho_1$. This is possible through a downward vertical line (similar to path 2d) and then a continuously decreasing part (2e) along the $\rho^*_{2-}$ branch. Path 2d is a downward shock that is shown in Figs. 9(b) and 9(c). In the case where the density varies along lines (3c) and (3d), we have a downward boundary layer near $x = 1$. These possibilities are expected if $\alpha_1$ is increased further from its value that leads to 2c- and 2d-type variations. As before, the principle is that if the 3d-type vertical line intersects the $\gamma_1$ line before reaching the $\rho^*_{2-}$ branch, the 3d-type line represents a boundary layer satisfying the boundary condition at $x = 1$. If the reverse happens, this downward vertical line represents a downward shock at the bulk which needs to be followed by a continuously decreasing density part along the $\rho^*_{2-}$ branch. This is a general principle which can be applied to other cases also to see the deconfinement of a boundary layer giving rise to a shock in the bulk (see Ref. [8]).

With a further increase in $\alpha_1$, the density variation from the $x = 0$ end is still the same as before up to part 3c along the $\rho^*_{2+}$ curve, except that now the density approaches $\rho^{*+}_{1m}$ more closely along the 4c-like path. Finally, for a given $\alpha_1$, the density reaches the value $\rho^{*+}_{1m}$. After this, the boundary condition is satisfied through a depleted boundary layer represented by vertical path 4d. With a further increase in $\alpha_1$, the density cannot now go around $\rho^{*+}_{1m}$ to move to the $\rho^*_{1+}$ branch due to the constraint from the stability property. In that case, the only option for the density is to proceed along line (4c) but to move to the $\rho^*_{1+}$ branch along a vertical line similar to (5d) before reaching the point $\rho^{*+}_{1m}$. There is now a second high-density upward shock in the density profile at larger $x$ [line (5d)], with the first shock being a low-density one represented by line (2b). With an increase in $\alpha_1$, the 5d-type vertical line moves to higher values of $C_0$. The boundary condition at $x = 1$ is now satisfied by the rest of the density profile, where the density decreases continuously along path (5e) to the minimum $\rho^{*+}_{1m}$ and then decreases through a depleted boundary layer represented by line (4d). Thus, for example, for this value of $\alpha_1$, we see the following parts in the density profile as we move along the density profile from its $x = 0$ end. (i) First is a continuously varying density profile that satisfies the boundary condition $\rho(x = 0) = \alpha_1$. (ii) This is followed by a low-density upward shock of maximum height connecting $\rho_{1l} = \rho^{*-}_{10}$ and $\rho_{1r} = 0$. (iii) Beyond this shock, there is again a continuously increasing part. (iv) This is followed by an upward, high-density shock. (v) Beyond this high-density shock, the density decreases continuously to $\rho^{*+}_{1m}$. (vi) The last part is a particle-depleted boundary layer, which saturates to $\rho^{*+}_{1m}$ for $x < 1$ and satisfies the boundary condition at $\rho_1(x = 1) = \gamma_1$. All these features can be verified from the density profiles in Fig. 9.

If $\alpha_1$ is increased further, the upward high-density shock [vertical lines like (5d)] will move toward higher $C_0$ values. For certain $\alpha_1$, the low- and the high-density shocks merge and there is a big symmetric shock with $C_0 = 0$. Beyond this $\alpha_1$, the big upward shock persists, and this is followed by a continuously varying part [similar to line (1c)] along which the density decreases and approaches $\rho^{*+}_{1m}$. The boundary condition is again satisfied by the particle-depleted boundary layer represented by line (4d).

## V. SHOCKS AND BOUNDARY LAYERS: Boundary conditions and saturation properties

Since boundary layers and shocks are the special features through which various density distributions are distinguished, our general predictions are more on different kinds of boundary layers and shocks rather than the bulk profiles. In the following, we discuss the boundary conditions for the occurrence of different kinds of shocks and the nature of the saturation of shocks or boundary layers to special bulk densities which correspond to different bifurcation points in the fixed-point diagram.

### A. Boundary conditions

Inferences related to the boundary conditions are drawn from the detailed analysis of the previous section based on the

fixed-point diagram in Fig. 5. This diagram helps us identify shocks or boundary layers that are consistent with the boundary conditions as well as the stability properties of the fixed points.

(1) *Downward shock in the bulk or a particle-depleted boundary layer at* $x = 1$. Either of these features appears whenever the density profile decreases through a jump discontinuity from the $\rho^*_{2+}$ branch to the $\rho^*_{2-}$ branch or from $\rho^{*+}_{1m}$ to $\rho^{*-}_{1m}$. The condition for this is $\gamma_1 < \rho^{*+}_{1m}$. The value of $\alpha_1$ is somewhat flexible since it is possible to see these features both for $\alpha_1$ positive and for $\alpha_1$ negative.

(2) *Upward symmetric shock in the bulk or depleted boundary layer at* $x = 0$. This is seen whenever the density profile jumps from $\rho^*_{1-}$ to $\rho^*_{1+}$. This happens for various combinations of $\alpha_1$ and $\gamma_1$ such as $\alpha_1 < 0$ or $\alpha_1 > 0$ with $\gamma_1 > \rho^{*+}_{1m}$ or $\gamma_1 < \rho^{*+}_{1m}$. At $x = 0$, the density profile may start with a continuously varying part followed by a symmetric large shock, or it can satisfy the boundary condition at $x = 0$ with the help of a boundary layer. In both cases, the discontinuity in the density corresponds to a discontinuous jump from $\rho^*_{1-}$ to $\rho^*_{1+}$.

The presence or absence of a boundary layer at $x = 0$ is specified completely by the value of $C_0$ at $x = 0$. Let us assume that $\rho_1 = \alpha_1$ line intersects the curve in Fig. 5 at a value $C_0 = C_0(\alpha_1)$. A condition such as $C_0(\alpha_1) = C_0(x = 0)$ would mean a continuously varying density near $x = 0$. If these two values are unequal, it would imply the presence of a boundary layer. For example, for $\alpha_1 > \rho^{*+}_{1m}$, a particle-rich or a particle-depleted boundary layer appears if $C_0(\alpha_1) > C_0(x = 0)$ and $C_0(\alpha_1) < C_0(x = 0)$, respectively. However, it is important to pay attention to certain situations which are forbidden due to the stability properties. For example, if $\alpha_1 < \rho^{*-}_{1m}$, a boundary layer with $C_0(x = 0) < C_0(\alpha_1)$ is not possible.

(3) *Double shock*. In this case, the density profile has both high- and low-density upward shocks, with the low-density shock having maximum possible height $\rho^{*-}_{10}$. To have a high-density shock, the lower end of the high-density shock must be on the $\rho^*_{2+}$ branch. The density can reach this branch only via $\rho_1 = 0$ point. The only way the density can reach the $\rho_1 = 0$ point is through a low-density shock represented by the $C_0 = 0$ line across the negative lobe. A low-density shock representing a jump across the negative lobe along $C_0 = 0$ line has the maximum possible height.

A density-profile with a double shock may appear for $\alpha_1 < \rho^{*-}_{1m}$ and $\gamma_1 < \rho^{*+}_{1m}$ or $\gamma_1 > \rho^{*+}_{1m}$. In the case of $\gamma_1 > \rho^{*+}_{1m}$, the density after the high-density shock varies continuously along the $\rho^*_{1+}$ branch to satisfy the boundary condition at $x = 1$. For $\gamma_1 < \rho^{*+}_{1m}$, the second shock is possible for some $\alpha_1$. In this case, after reaching the $\rho^*_{1+}$ branch, the density decreases till $\rho^{*+}_{1m}$ and then decreases further as a depleted boundary layer at $x = 1$ to satisfy the boundary condition.

It is interesting to note that although it is possible to have a profile with only a low-density shock, the same with a single high-density shock is never possible. The flow behavior suggests that a high-density shock has to be always accompanied by a low-density shock of maximum height.

(4) *Boundary layer at* $x = 1$. As in the case of a boundary layer at $x = 0$, it is also possible to specify the conditions for a boundary layer at $x = 1$ by comparing the value of $C_0(x = 1)$ with $C_0(\gamma_1)$. In general, a boundary layer will appear at $x = 1$ if these two values of $C_0$ are different. As an example, a downward boundary layer for $\rho^{*-}_{1m} < \gamma_1 < \rho^{*+}_{1m}$ appears if $C_0(x = 1) < C_0(\gamma_1)$.

### B. Saturation of the shock

From Eq. (13), we find that near the saturation to a bulk density $\rho_{1b}$, the slope of the boundary layer is given by

$$\frac{d\delta\rho_1}{d\tilde{x}} = \left(\frac{|\,r\,|}{2} - \frac{u}{2}\rho^2_{1b}\right)\rho_{1b}\delta\rho_1, \tag{22}$$

where it is assumed that the boundary-layer density is $\delta\rho_1$ away from the saturation value, $\rho_{1b}$. This shows that the saturation of the boundary layer to the bulk is, in general, exponential except for three special points. The saturation is of power-law kind, if $\rho_{1b} = 0$ or $\rho_{1b} = \rho^{*\pm}_{1m} = \pm(\frac{|r|}{u})^{1/2}$. The length scale associated with the exponential approach of the shock to the bulk density diverges as the bulk density approaches these special values. As discussed in Sec. II C, the critical points correspond to special boundary conditions $(\alpha_c, \gamma_c)$ at which the shock height across the positive or negative lobe decreases to 0. Therefore, the approach to the critical point is associated with the continuous vanishing of the shock height along with the divergence of the length scale over which the shock saturates to the bulk.

## VI. SUMMARY

Here, we have considered a driven diffusive process of interacting particles on a finite, one-dimensional lattice. These particles have mutual repulsion in addition to the mutual exclusion interaction. Apart from the hopping dynamics of the particles, the model also has particle attachment-detachment processes, which lead to particle nonconservation in the bulk. Such driven particle systems are known to exhibit boundary-induced phase transitions for which the tuning parameters are the boundary densities $\alpha$ and $\gamma$. In different phases, the average particle density distributions across the lattice have distinct shapes, with various types of discontinuous jumps from one density value to another. Here, we carry out a phase-plane analysis for the boundary-layer differential equation to understand how the fixed points of the boundary-layer equation and their flow properties determine the shape of the entire density profile under given boundary conditions. Such a fixed-point analysis has been very useful in understanding the phases and phase transitions of particle conserving models for which the constant bulk density values in different phases are given by the physically acceptable fixed points of the boundary-layer equation. In addition, the number of steady-state phases, the nature of the phase transitions, and the locations of the boundary layers can be obtained analytically from the phase-plane analysis of the boundary-layer equation. Results obtained upon applying this method to a particle conserving two-species process [14] show agreements with numerical simulations [15]. The present work provides a generalization of the method to a particle nonconserving process.

To apply this method, we have considered the hydrodynamic limit of the statistically averaged master equation describing the particle dynamics. The hydrodynamic equation, describing the time evolution of the average particle density $\rho$, looks like a continuity equation supplemented with the

particle nonconserving terms. The current contains the exactly known hopping current and a regularizing diffusive current part. The boundary-layer equation, which is the main focus of this work, can be obtained from the particle conserving part of the hydrodynamic equation. For convenience, we use $\rho_1 = 2\rho - 1$ for the boundary-layer equation. $\rho_1$ is related to the deviation from $\rho = 1/2$ (half-filled case).

It is found that the fixed points, $\rho_1^*$, of the boundary-layer equation are determined in terms of a parameter $C_0$ related to the excess current measured from $\rho = 1/2$ (half-filled case). Since the fixed points are dependent on $C_0$, one can plot the physically acceptable fixed points as a function of $C_0$ on the $C_0$-$\rho_1^*$ plane. In the steady state, the constancy of the current across a shock or a boundary layer implies that such objects can be represented by a fixed value of $C_0$. The boundary layers or shocks of the density profiles are represented by the constant-$C_0$ lines on this $C_0$-$\rho_1^*$ plot. The densities at which the constant-$C_0$ line intersects the fixed-point branches are the densities to which the shock or the boundary layer saturates. The discontinuous change in the density has to be consistent with the stability properties of the fixed points. For given values of $\alpha$ and $\gamma$, we can start from the $x = 0$ end of the density profile and find out how the density can change along the profile as it proceeds to satisfy the boundary condition at $x = 1$. This density variation along the density profile can be conveniently marked on the $C_0$-$\rho_1^*$ plot to see its consistency with the flow properties of the fixed points. Our approach does not give any information about the location of a shock since it does not involve the details of the bulk part of the profile. Instead, it is found that the conserved quantity $C_0$ plays an important role in deciding the shape of the density profile.

The emphasis of our approach is on the boundary-layer equation, which appears to control the shape of the entire density profile. In a sense, this approach is like holography, where the zero-dimensional boundary can help in building the bulk one-dimensional density profile. Particle nonconserving processes are not important for the boundary layers. This simplicity allows us not only to classify different kinds of density distributions, but also to gain more physical insight as to why some features of the density profile are evident under certain boundary conditions. Some of these features are mentioned below.

(1) When a density profile has two shocks, the low-density shock is of maximum possible height. For given values of the interaction parameters, the height of the low-density shock can be obtained explicitly.

(2) It is possible to have a low-density shock alone in the profile but a high-density shock has to always be accompanied by a low-density shock of maximum height.

(3) A downward shock is produced by the deconfinement of a downward boundary layer at $x = 1$. The condition on $\gamma$ for seeing a downward shock or a downward boundary layer at $x = 1$ can be precisely specified.

(4) The symmetric two-peak structure of the current as a function of the particle density is responsible for a symmetric two-lobe structure of the fixed points drawn on the $C_0$-$\rho_1^*$ plane. The flow behavior of the fixed points around the two lobes is asymmetric. This is the reason why the two critical points in the phase diagram are not symmetrically related to each other. This asymmetry is reflected in the shapes of the density profiles near these critical points.

(5) For a given boundary condition, a density profile with only one boundary layer and no shock can be fully specified by the value of $C_0$ at this end.

In addition to these issues, this analysis also provides quantitative predictions regarding the heights of different kinds of shocks. There can be other length scales related to the crossover of the shock (or the boundary layer) to the bulk and to the deconfinement of the boundary layer from the boundary to form a shock [8]. The critical properties of the boundary-induced phase transitions can be characterized through these length scales. As we have shown here, shocks saturating to special bifurcation densities have diverging crossover length scales.

The generality of the fixed-point-based boundary-layer analysis suggests its wider applicability to other problems where boundary layers play an important role in the entire distribution. The method relies on the hydrodynamic equation, and the solution is exact to the extent to which the hydrodynamic equation is exact. Needless to say, this method can be readily used for various other driven exclusion processes for which the current-density relationships either are known or can be determined accurately.

## ACKNOWLEDGMENTS

Financial support from the Department of Science and Technology, India, and the warm hospitality of ICTP (Italy), where the work was initiated, are gratefully acknowledged.

## APPENDIX: SHOCKS FOR VARIOUS $C_0$

Figure 5 shows the dependence of the fixed points on the parameter $C_0$ and, in particular, the saddle-node bifurcation in which the fixed points are usually created or destroyed with the variation of the parameter. Since $C_0$ can be expressed purely in terms of $J$, with its constant parts subtracted, it remains constant across a shock or a boundary layer. In this Appendix, we discuss how different values of $C_0$ determine different kinds of shocks in this system.

In principle, using Eq. (14), one can obtain the value of $C_0$ along the continuously varying parts of the density profile. Hence, as we move along a density profile having bulk shocks, $C_0$ changes per Eq. (14) along the outer solution parts of the profile with intermediate constant values across the shock or inner solution regions. The value of $C_0$ in the shock region is fixed by one of the bulk density values to which the shock saturates.

Let us assume that the shocks or the boundary-layer approach the bulk densities $\rho_{1r}$ or $\rho_{1l}$ as $\tilde{x} \to \pm\infty$, respectively. Since $\rho_{1l}$ and $\rho_{1r}$ are various fixed points of the inner equation, the approach to these fixed points has to be consistent with the flow properties. A shock is called an upward shock if $\rho_{1l} < \rho_{1r}$. The reverse, that is, $\rho_{1l} > \rho_{1r}$, is true for a downward shock.

(1) $C_0 > 0$. In this case, there are two fixed points $\rho_{1+}^*$ and $\rho_{1-}^*$ symmetrically located about $\rho_1 = 0$, with $\rho_{1-}^*$ being an unstable fixed point. Thus if a shock is formed with $C_0 > 0$, it should be an upward shock which approaches the fixed points

$\rho_{1r} = \rho^*_{1+}$ and $\rho_{1l} = \rho^*_{1-}$ as $\tilde{x} \to \infty$ and $-\infty$, respectively. The shock height, in this case, is $\rho^*_{1+} - \rho^*_{1-}$.

(2) $C_0 < 0$. In this case, four fixed points lead to different kinds of shocks.

(a) It is possible to see a downward shock with $\rho_{1l} = \rho^*_{2+}$ and $\rho_{1r} = \rho^*_{2-}$. The downward shock is thus symmetric about $\rho_1 = 0$. The flow in Fig. 4 shows that a downward shock cannot involve other fixed points since that would not be consistent with the stability criteria of the fixed points.

(b) There can be small upward shocks which lie entirely in the range $\rho_1 > 0$. We have already referred to these shocks as high-density shocks. In terms of the fixed points, the left and right saturation densities of the shock are $\rho_{1l} = \rho^*_{2+}$ and $\rho_{1r} = \rho^*_{1+}$, respectively.

(c) The third possibility is that of an upward shock entirely in the $\rho_1 \leqslant 0$ range. Such a shock has been referred to as a low-density shock. For this shock, $\rho_{1l} = \rho^*_{1-}$ and $\rho_{1r} = \rho^*_{2-}$.

(3) $C_0 = 0$: There can be an upward shock with $\rho_{1r} = 0$ and $\rho_{1l} = \rho^*_{1-}$. There can also be an upward shock connecting the densities $\rho_{1l} = 0$ and $\rho_{1r} = \rho^*_{1+}$. These two shocks together appear as a large shock, symmetric around $\rho_1 = 0$.

Alternatively, different kinds of shocks can tell us the range of values for $C_0$.


[1] T. M. Liggett, *Interacting Particle Systems: Contact, Voter and Exclusion Processes* (Springer-Verlag, Berlin, 1999); R. B. Stinchcombe, J. Phys. Condens. Matter **14**, 1473 (2002).

[2] D. Helbing, Rev. Mod. Phys. **73**, 1067 (2001).

[3] S. Katz, J. L. Lebowitz, and H. Spohn, J. Stat. Phys. **34**, 497 (1984).

[4] J. S. Hager, J. Krug, V. Popkov, and G. M. Schütz, Phys. Rev. E **63**, 056110 (2001).

[5] J. Krug, Phys. Rev. Lett. **67**, 1882 (1991).

[6] A. B. Kolomeisky, G. M. Schütz, E. B. Kolomeisky, and J. P. Straley, J. Phys. A **31**, 6911 (1998).

[7] A. Parmeggiani, T. Franosch, and E. Frey, Phys. Rev. E **70**, 046101 (2004); M. R. Evans, R. Juhász, and L. Santen, *ibid.* **68**, 026117 (2003).

[8] S. Mukherji and S. M. Bhattacharjee, J. Phys. A **38**, L285 (2005); S. Mukherji and V. Mishra, Phys. Rev. E **74**, 011116 (2006).

[9] S. Mukherji, Phys. Rev. E **76**, 011127 (2007).

[10] V. Popkov, A. Rákos, R. D. Willmann, A. B. Kolomeisky, and G. M. Schütz, Phys. Rev. E **67**, 066117 (2003).

[11] S. M. Bhattacharjee, J. Phys. A **40**, 1703 (2007).

[12] J. Maji and S. M. Bhattacharjee, Europhys. Lett. **81**, 30005 (2008).

[13] J. D. Cole, *Perturbation Methods in Applied Mathematics* (Blaisdell, Waltham, MA, 1968).

[14] S. Mukherji, Phys. Rev. E **79**, 041140 (2009).

[15] V. Popkov, J. Stat. Mech. (2007) P07003; V. Popkov and G. M. Schütz, *ibid.* (2004) P12004.

[16] S. H. Strogatz, *Nonlinear Dynamics and Chaos* (Perseus Books, Cambridge, 1994); R. Hoyle, *Pattern Formation: An Introduction to Methods*, 1st ed. (Cambridge University Press, Cambridge, 1996).